Combustion and Flame 156 (2009) 1594–1603

Contents lists available at ScienceDirect

Combustion and Flame

journal homepage: www.elsevier.com/locate/combustflame

Experimental and computational study of methane counterflow diffusion flames perturbed by trace amounts of either jet fuel or a 6-component surrogate under non-sooting conditions

H. Bufferand, L. Tosatto, B. La Mantia [1], M.D. Smooke, A. Gomez *

Department of Mechanical Engineering, Yale Center for Combustion Studies, Yale University, New Haven, CT 06520-8286, USA

ARTICLE INFO

Article history:
Received 19 August 2008
Received in revised form 16 December 2008
Accepted 4 March 2009
Available online 6 June 2009

Keywords:
Diffusion flame
Counterflow
Surrogate
Jet fuel

ABSTRACT

The chemical structure of a methane counterflow diffusion flame and of the same flame doped with 1000 ppm (molar) of either jet fuel or a 6-component jet fuel surrogate was analyzed experimentally, by gas sampling via quartz microprobes and subsequent GC/MS analysis, and computationally using a semi-detailed kinetic mechanism for the surrogate blend. Conditions were chosen to ensure that all three flames were non-sooting, with identical temperature profiles and stoichiometric mixture fraction, through a judicious selection of feed stream composition and strain rate. The experimental dataset provides a glimpse of the pyrolysis and oxidation behavior of jet fuel in a diffusion flame. The jet fuel initial oxidation is consistent with anticipated chemical kinetic behavior, based on thermal decomposition of large alkanes to smaller and smaller fragments and the survival of ring-stabilized aromatics at higher temperatures. The 6-component surrogate captures the same trend correctly, but the agreement is not quantitative with respect to some of the aromatics such as benzene and toluene. Various alkanes, alkenes and aromatics among the jet fuel components are either only qualitatively characterized or could not be identified, because of the presence of many isomers and overlapping spectra in the chromatogram, leaving 80% of the carbon from the jet fuel unaccounted for in the early pyrolysis history of the parent fuel. Computationally, the one-dimensional code adopted a semi-detailed kinetic mechanism for the surrogate blend that is based on an existing hierarchically constructed kinetic model for alkanes and simple aromatics, extended to account for the presence of tetralin and methylcyclohexane as reference fuels. The computational results are in reasonably good agreement with the experimental ones for the surrogate behavior, with the greatest discrepancy in the concentrations of aromatics and ethylene.

1. Introduction

With the general need for enhanced flexibility in the sources of fuels, it is becoming increasingly important to improve scientific knowledge of the combustion properties of practical fuels such as aviation kerosenes. Jet fuel is expected to continue to play a central role in both civilian and military aviation for the next several decades. A successful characterization of the fuel chemical kinetics, as achieved for simple molecules in the past several decades, would enable the development of reduced chemical kinetics that could be incorporated in quantitative models of gas turbines. This, in turn, will lead to improved engine efficiency and reduce pollutant formation.

There are a variety of challenges posed by numerical and experimental studies in aero-combustor systems. These include the hostility of the combustion environment in applying quantitative diagnostic techniques and the enormous computational resources required to "solve" the problem. In addition, the complex composition of real fuels containing hundreds of chemical species make their complete kinetic characterization and modeling an impractical prospect. For these reasons, this type of research ought to be pursued in simple combustion environments. Therefore, testing/modeling is typically performed in flow reactors, shock tubes and laminar flames that are well suited to the development of a chemical kinetic model because of their highly simplified fluid mechanics, as compared to practical, and inevitably turbulent, flames. Although stirred/flow reactors and shock tubes offer better controlled conditions for a rigorous characterization of the fuel chemical kinetic behavior, the ultimate test remains a flame environment, since it provides the critical coupling between chemical kinetics and transport that is relevant to all combustion applications. With respect to the composition challenge, the presence of a multitude of compounds in a typical kerosene suggests as a practical approach the identification of surrogate fuel mixtures, having only a small number of components, whose combustion behaviors

* Corresponding author. Fax: +1 203 432 7654.
E-mail address: alessandro.gomez@yale.edu (A. Gomez).
[1] Present address: Shell Exploration and Production Co., Two Shell Plaza, 777 Walker St, Houston, TX 77002, USA.

0010-2180/$ - see front matter © 2009 The Combustion Institute. Published by Elsevier Inc. All rights reserved.
doi:10.1016/j.combustflame.2009.03.006

capture essential features of those of the real fuels. This is the strategy that has been implemented in the combustion community for the past several years.

To date, candidate surrogates have been identified for kerosenes such as Jet A, for Fischer–Tropsch Jet A and for JP-8. The combustion properties of these surrogates have been compared successfully with those of the original fuels in some narrowly defined tests. The topic has been comprehensively reviewed by Dagaut et al. [1]. After an initial effort by Schultz [2] on the thermal and oxidative stability of a 12-component surrogate, the number of components in the surrogate has been decreasing to a more manageable six in the so-called Utah surrogate [3], five in the Drexel surrogate [4], and, most recently, to three in a joint contribution from the University of Milan and UC San Diego [5]. Also noteworthy is the recent work in a jet stirred reactor [6] that presents a comparison between jet fuel and a 3-component surrogate, with reasonable agreement between experimental and numerical results at pressures as high as 40 atm. Clearly, one has to define precisely the objectives. The oxidation behavior of kerosene may be even modeled with a single alkane, such as *n*-decane, if aromatic behavior is of no concern [6]. Otherwise, at a minimum, a mixture of alkanes and aromatics is necessary. A very recent study using a 2-component (80% decane and 20% 1,2,4-trimethylebenzene) Aachen surrogate [7] suggests that even such a simple formulation can mimic successfully flame speed, autoignition behavior, extinction in diffusion flame and even peak soot volume fraction of jet fuel flames.

These results are encouraging, but, at this stage, it is still not clear what is the minimum number of compounds necessary for a successful surrogate formulation and the answer is likely to depend on the definition of success. If the task is to mimic global properties such as extinction/ignition behavior and flame speed, a few components and highly reduced chemical kinetic mechanisms will probably suffice. If aromatic and soot production rate needs to be captured quantitatively, the answer is still unknown, although the study in [7] gives hope that even in such a case a simple formulation may suffice.

The present contribution builds on the research we began in collaboration with research groups at the University of Utah and at the University of Milan [8]. The task of the Milan group has been to provide the chemical kinetic model for a jet fuel surrogate involving, as mentioned earlier, typically a mixture of alkanes and aromatics. In their approach, the primary oxidation and decomposition reactions of reference components are automatically generated in a complete and detailed way. The complete scheme is then lumped and the reactions are grouped to obtain a semi-detailed or lumped kinetic scheme. This technique has been successfully applied and already partially validated for gasolines, *n*-heptane, *iso*-octane, *cyclo*-alkanes, aromatics and ethers [9].

In our earlier study [8], the emphasis was on validating the surrogate selection by matching overall combustion behavior such as the extinction strain rate and temperature profile in diffusion flames. This goal was successfully reached with a 6-component surrogate with the same components as the Utah surrogate [3], that had been designed to match the volatility of the jet fuel and its overall sooting behavior based on smoke tests. Now, the focus is shifted to the validation of this surrogate with respect to diffusion flame structure, with a comprehensive chemical characterization of the flame by gas sampling through quartz microprobes and analysis by standard analytical chemistry techniques such as GC/MS. Counterflow flames are considered since they provide the simplest one-dimensional environment for concurrent detailed modeling. Initial experimental data on a similar flame were discussed in [10]. Here attention is focused on a methane baseline flame that can be stabilized and modeled independently of the liquid fuel perturbation, to track the effect of the liquid fuel addition all the way to C2 species by sorting out the baseline flame contribution to these species. Furthermore, we model computationally the flame with the semi-detailed chemical kinetic mechanism. In addition to attempting to validate the surrogate formulation with respect to the flame structure, the objective is also to provide a database for the pyrolysis and oxidation behavior of jet fuel in a diffusion flame for other investigators to use in parallel research efforts in this area.

2. Experimental setup

The experimental setup consists of a counterflow burner [8]. A nitrogen shroud shields the flame from room drafts and ensures burning only in the controlled atmosphere that is determined by the composition of the feed streams. Fig. 1 shows a schematic of the experimental set-up. Obtaining complete vaporization of the fuel is one of the critical issues when dealing with mixtures of heavy hydrocarbons, since fractional distillation may occur. Previous work used an ultrasonic atomizer to nebulize the fuel in very small droplets. This system is now upgraded by using an electrospray [11], which provides greater flexibility in flow rates, without

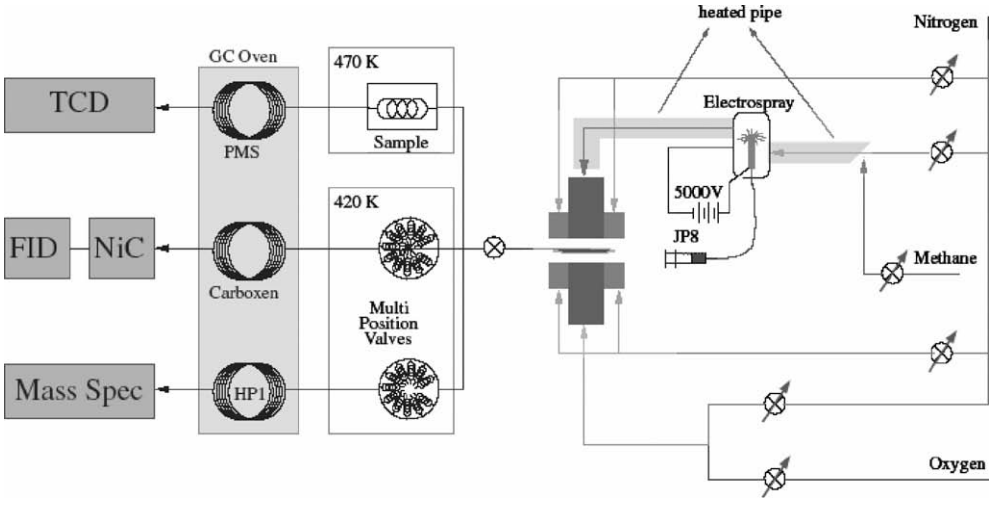

Fig. 1. Schematic of the experimental setup.

compromising the stability of the flame. To ensure complete fuel evaporation and prevent condensation downstream of the electrospray unit, PID controllers keep the fuel line at 430 K, which is well above the dew point of the liquid-fuel/CH_4/N_2 mixture. Samples of the gas are extracted from the flame through a small silica probe. This probe has an outer diameter of 340 μm and an inner diameter of 170 μm, which yields adequate spatial resolution during the flame sampling and minimizes the flame perturbation, as demonstrated by comparison with a much smaller probe used in earlier work [10].

The jet fuel was provided by Wright–Patterson Air Force Base (POSF No. 4658). To account for the considerable variability in the composition of jet fuel from different refineries, an "average" jet fuel was synthesized by mixing together 5 Jet A fuels from different U.S. manufacturers. The composition of that blend in vol% is: 55.2% paraffins (*n*- and *i*-), 17.2% monocycloparaffins, 12.7% alkyl benzenes, 7.8% dicycloparaffins and 4.9% indans and tetralins. The balance, ≈ 2%, is in naphthalenes and trycylcoparaffins. The surrogate is the 6-component blend of well-known hydrocarbons as used in [8], with the following molar composition: 10% *iso*-octane (C_8H_{18}), 20% methylcyclohexane (C_7H_{14}), 15% *m*-xylene (C_8H_{10}), 30% *n*-dodecane ($C_{12}H_{26}$), 5% tetralin ($C_{10}H_{12}$), and 20% tetradecane ($C_{14}H_{30}$). This surrogate has the same components as the Utah surrogate [3], but the above-mentioned percentages are on a *molar* basis rather than in volume percent, which amounts to a lower concentration of aromatics and larger concentration of aliphatics as compared to the composition of the Utah surrogate. We will refer to it as the Utah/Yale surrogate in the remainder of the article. Preliminary experiments showed some evidence of condensation in the unheated probe at some positions near the fuel outlet. In part for this reason, the fuel in the liquid phase is added in trace amounts to a baseline methane flame, as further elaborated below. Since the dispersion of the liquid hydrocarbons into fine droplets was implemented by an electrospray, which requires a liquid of finite electric conductivity, both jet fuel and surrogate were doped with 0.05% (by volume) of an antistatic additive, Octel Stadis 450. This additive is already present in JP-8 and may be present in Jet A at concentrations up to 80 ppm.

The chemical analysis is performed by a gas chromatograph (Agilent 6890A) equipped with thermal conductivity (TCD), flame ionization (FID) and mass spectrometry detectors (MSD) (Agilent 5973N). The instrument is capable of quantifying complex hydrocarbon mixtures, CO and CO_2. The GC/MSD uses two columns, a Supelco Carboxen and an Agilent HP-1, connected to the FID and MSD, respectively. In addition, the TCD measures non-hydrocarbon stable gases separated by means of a third column (Alltech, Packed Molecular Sieve). Because of its much wider linear range, this detector is better suited than the MSD for the analysis of gases present as large fractions of the gas sample and/or in greatly varying amounts. A homemade Nickel-based catalytic converter (Methanizer) allows for FID quantification of CO and CO_2 upon their conversion into methane in the presence of hydrogen. The system can separate and quantify N_2, O_2, CO, CO_2, light gaseous hydrocarbons and higher hydrocarbons up to C_{14}, and even higher.

The GC data are post-processed by identifying the species by both the column retention time and the molecule specific spectrum. GC/MS analysis produces a wealth of information but has one main drawback: it takes a very long time to complete an analysis. A concentration measurement at any point in the flame typically requires: 5 min to load the sample loop, 2 min for the analysis of O_2 and N_2 by the TCD, 25 min for the analysis of light (C1 and C2) species by the FID and at least one hour for the analysis of large molecular-weight compounds via MS. Clearly, a full flame dataset with a minimum of 10–12 points would entail a tedious procedure lasting in excess of 30 h. Preserving a steady flame over such a time would be challenging, especially in the case of jet fuel that requires precise metering of liquid flow rates. Using a syringe pump, as is typically done at the small flow rates of interest, would entail repeated flame shut-offs with reloading of syringes. If one factors in thermal transients of the burner and other inevitable variabilities, for example, sampling probe distortions through flame start up and shut down over a 30 h time period, the potential for reproducibility problems in the measurements is high.

To ease the protocol of the chemical analysis, an automated sampling system was developed, along the lines of [12] to allow for sampling/storing using two multiposition valves, two pneumatic-actuated injection valves and a battery of sampling loops, as shown in Fig. 1. One of the pneumatic valves is responsible for the TCD analysis (top left in the figure) that is executed in real time, since it requires only 2 min per data point. The other valve, on the other hand, controls the FID and the MS. Since these two instruments require a much longer time to complete a measurement, the samples are stored at 423 K in two sets of 16 sample loops using other two multi-position valves and analyzed overnight by a computer-automated sequence. Thanks to this improvement, collecting samples from a flame requires at most three hours of operator work during which the flame has to run continuously. This dramatic gain in the implementation of the experiment opens the doors to the systematic study of flame structures with relative ease.

The overall accuracy of the chemical analytical instrument has been assessed both by analyzing gas mixtures of known composition, to evaluate potential bias errors, and by repeated sampling at the same position in the flame, to estimate the precision error. The peak areas of the chromatograms show good repeatability within ±4% confirming the adequacy of the above-described sampling system. Another source of uncertainty is the calibration: for small molecules, calibrated gas mixtures (SCOTTGAS®) are used; for the heavier species, liquid solutions of acetone and carefully measured aliquots of each component are prepared and injected in the GC/MS. The total error is estimated at 7% for light species and 12–15% for the heavier ones.

Temperature measurements were performed using flame-welded, silica coated Pt–10%Rh/Pt thermocouples with a typical junction diameter measuring on the order of 70 μm. Standard corrections for radiative losses were applied.

A non-intrusive laser diagnostics measurement was performed in one of the flames to assess the perturbation of the sampling probe and to justify a possible shift between experiments and computation due to probe artifacts. To measure OH by Planar Laser Induced Fluorescence (PLIF), a 2 mJ UV laser beam from a frequency-doubled Nd–Yag pumped dye laser was tuned to excite the $Q_1(8)$ transition of the (1,0) band of the $A^2\Sigma^+ \leftarrow X^2\Pi$ system at a wavelength of 283.5 nm. The beam was expanded and shaped into a laser sheet by a 300 mm cylindrical quartz lens. The fluorescence signal at 310 nm was imaged on a 1280 × 1024 ICCD camera (Cooke Dicam-Pro series) through a UV-Nikkor 105 mm f/4.5 UV lens.

3. One-dimensional computational model

The form of the governing equations for the counterflow flame model is well documented and presented in detail elsewhere (see, e.g., [13,14]). The counterflow problem is modeled by considering a similarity solution of the two-dimensional conservation equations of mass, momentum, species and energy, valid along the stagnation point streamline. The resulting set of equations can be written in terms of a nonlinear boundary value problem on a fixed spatial domain. Submodels for the thermodynamic and transport quantities, the chemistry and the divergence of the radiative flux are evaluated using highly optimized libraries [15] and an optically thin

radiation model [16]. Despite the significant variations in the molecular weight of the species, Ludwig–Soret effects, driving light molecules towards higher temperature regions and heavier molecules towards colder temperature regions [17], were not included and may have to be incorporated in future refinements. In all cases, the software developed at Yale is used to study these problems on machines that include an 8-cpu AMD Opteron cluster equipped with 32 GB of RAM and two four-way IBM 44P-270 systems running Linux. All computational systems are connected to a high-speed 1.2 TB RAID array via gigabit Ethernet links. Of inherent importance to the nonpremixed studies is the ability to vary one or more quantities studied in the experiments, as the remaining system parameters are held fixed. For example, in the diffusion flames, the strain rate, inlet mass flow rates and temperatures are parameters of interest. We apply a continuation method such that the grid and the solution smoothly change as the parameter is varied. Specifically, the solution algorithm we implement utilizes a phase-space, pseudo-arclength continuation method with Newton-like iterations and global adaptive gridding [18,19]. A semi-detailed kinetic mechanism for the surrogate blend is used for all flame calculations and is based on an existing hierarchically constructed kinetic model for alkanes and simple aromatics extended to account for the presence of tetralin and methylcyclohexane as reference fuels, as in our previous work [8].

4. Criterion for flame comparison

There are several options to choose from to compare flames with different composition. The overall objective is to use the flame as a well-controlled chemical reactor. In principle, it is advantageous to use a baseline flame, such as a methane diffusion flame as a reference with a prescribed velocity and thermal field, and then to perturb such a flame with known amounts of either jet fuel or surrogates. This approach, advocated by Hamins et al. [20] and, more recently, by McEnally et al. [21], has the following advantages: (i) it minimizes the potential of vapor condensation since the partial pressure of the condensable components is very modest; (ii) critical (non-chemical) variables, such as temperature and velocity, can be measured once and for all on the baseline flame, without the need of repetitious measurements on each chemically perturbed flame; (iii) probe-induced perturbation can be studied systematically on the simple baseline flame, since the fluid dynamic interaction of the intrusive probe and the flame is the same as when an additive is introduced. Residence time and temperature can be controlled by the flame strain rate and by the feed stream composition, respectively. Also, the jet fuel surrogate overall heat release behavior was successfully validated in [8], which is another reason why a self-sustained jet fuel flame is not indispensible and the perturbation approach is preferable.

Once this approach is chosen, clearly there are many degrees of freedom to ensure that the comparison between the baseline flame and the perturbed one is "fair." To control the flame temperature and prevent soot formation, the flame is highly diluted with nitrogen. To have measurable concentration of chemical species from the flame dopants, the concentration of jet fuel needs to be sufficiently large so that any species of interest must be produced in sufficiently large amounts to be able to distinguish it from the contribution from the background methane flame. Preliminary experiments showed that the additive must be in molar concentrations on the order of at least 1000 ppm. Such an amount corresponds to an energetic increment over the base-line methane flow rate on the order of 7%. As a result, the peak temperature may increase by 50–70 K and the location of the flame may shift slightly toward the oxidizer side. To maintain the same temperature profiles of the baseline flame, one could increase the inert molar fraction in either one of the two streams or both. Both changes may lead to a further shift of the flame towards the oxidizer side. However, these shifts may be compensated by a small increase in the flow rate on the oxidizer stream to move the stagnation flame in the opposite direction – towards the fuel side. In summary, by slightly adjusting feed stream composition, strain rate and mass flux at the burner outlets one can ensure that the following two conditions are fulfilled: the same temperature profile is maintained in the flames; and the stoichiometric mixture fraction, z_f, defined as

$$z_f = \frac{1}{1 + s\frac{Y_{FF}}{Y_{OO}}}, \tag{1}$$

is unchanged, at $z_f = 0.76$, where s is the stoichiometric mass ratio of oxygen to fuel, that in the case of jet fuel is assumed to have a molecular composition equivalent to $C_{11}H_{21}$, Y_{FF} and Y_{OO} are the feed stream mass factions of fuel (regardless of the chemical composition) and oxygen, respectively. Since temperature is the most critical variable in high activation energy chemistry that is typical of combustion, the first condition suggests that the Arrhenius kinetics can be properly compared between the two flames. The second condition suggests that, in the first approximation, the flame position with respect to the gas stagnation plane is unaltered by the perturbation, since the mixture fraction is a monotonic function of the axial position.

Table 1
Boundary conditions.

		Flame A	Flame B	Flame C
Fuel side	Molar composition			
	N_2	0.897	0.902	0.902
	CH_4	0.103	0.097	0.097
	C2–C5 alkane impurities	232 ppm	218 ppm	218 ppm
	Jet fuel ($C_{11}H_{21}$)		992 ppm	
	Methyl-cyclohexane			200 ppm
	iso-Octane			100 ppm
	m-Xylene			150 ppm
	Tetraline			50 ppm
	Dodecane			300 ppm
	Tetradecane			200 ppm
	Mass flux (g/min/cm^2)	2.80	2.97	2.97
	Temperature (K)	379	379	379
Oxidizer side	Molar composition			
	N_2	0.227	0.227	0.227
	O_2	0.773	0.773	0.773
	Mass flux (g/min/cm^2)	3.19	3.42	3.42
	Temperature (K)	340	340	340
	Strain rate (s^{-1})	134	144	144
	z_f	0.76	0.76	0.76

Table 1 specifies the density corrected strain rate [22], and the boundary conditions with mole fractions, total mass flux and outlet temperatures of both fuel and oxidizer streams for the three flames under consideration: the baseline CH_4 flame – Flame A, the jet fuel doped methane flame – Flame B, and the Utah/Yale surrogate-doped methane flame – Flame C. The inner diameter of the burner outlets is 12 mm and the burner separation is kept at 14.1 mm. Because of impurities in the CH_4 supply, trace amounts of C2–C5 alkanes were revealed by chromatographic analysis, the sum of which averages at approximately 225 ppm. The presence of these impurities did not prevent us from quantifying the jet fuel and surrogate perturbations.

5. Results and discussion

5.1. Major species and temperature

Figs. 2–8 show comparisons of species and temperature profiles among the various flames analyzed here. The experimental data

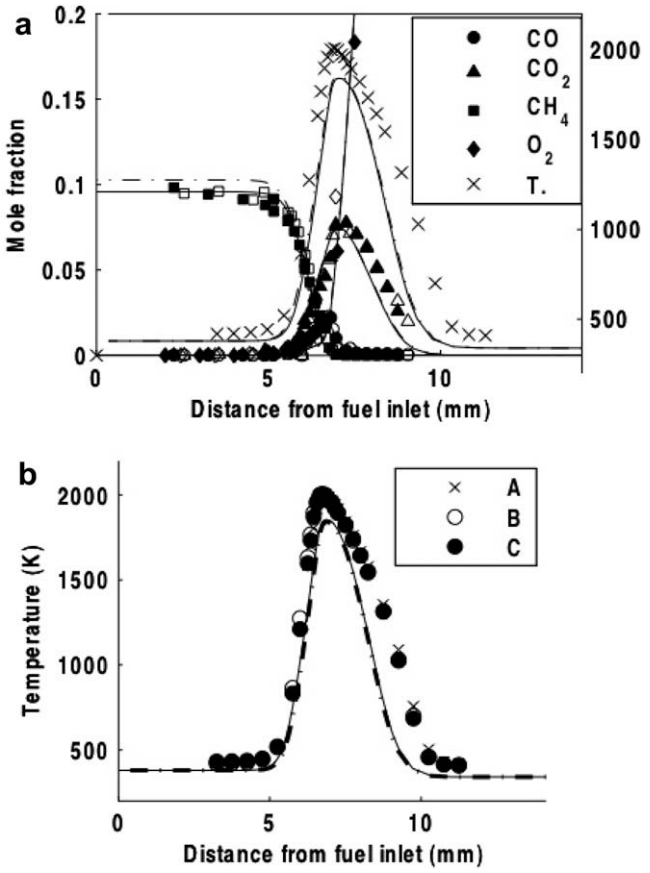

Fig. 2. (a) Comparison of some major species and temperature profiles of Flame B (full symbols) and Flame C (open symbols (experimental), dash/dot line (computational)), solid line (computational, Flame A); b) temperature profiles (same symbols as in a)). The ordinate scale does not allow for the presentation of all the data for O_2 up to the mole fraction (0.78) at the oxidizer boundary.

are shifted towards the oxidizer side by approximately 2 mm to account for three effects. The first is related to the nitrogen shroud. In the absence of such a shroud, the flame tends to be too sensitive to room drafts. In addition, towards its periphery it bends into a capped shape towards the fuel side. As a result, even when sampling regions at relatively low temperatures near the fuel mouth, where significant amounts of large species are present, the sampling probe necessarily crosses the flame, which may lead to probe artifacts such as the fouling of the probe interior by a brownish tar-looking compound, as observed in some preliminary experiments. To avoid this problem, the shroud flow was balanced in such a way to ensure flatness of the flame even at its periphery. This in turn required a larger flow rate from the nitrogen shroud on the fuel side of the burner as compared to that from the oxidizer side, which lead to a shift of the position of the flame by approximately 1 mm towards the fuel side. This arbitrary shift is obviously not accounted for in the one-dimensional simulation and requires a correction. There is a second, smaller shift between experimental data and simulation that is more difficult to quantify. It is related to the probe intrusiveness and its magnitude depends on the probe position, as further elaborated in Section 5.8. The third effect is a likely mismatch between experiments and computation in the velocity boundary conditions, that are specified on the basis of the mass fluxes and the temperatures at the boundaries (see Table 1). No velocity measurements were performed. It is well-known that regardless of how careful one is in the of design of the burner, even an axial velocity profile at the burner mouth that is top-hat in the jet configuration presents wings at the edges when mounted in counterflow. Consequently, the velocity at the centerline is slightly different from the mass-averaged velocity. Another difference in the velocity profile lies in the gradients at the boundaries that may vary from plug flow to potential flow and may result in an additional shift of the flame.

Fig. 2a shows a comparison of the experimental data among Flame B, Flame C and the computational results for Flames A and C. The simulation of the undoped Flame A is shown with a solid line, whereas that of the surrogate-doped Flame C with a dash–dot line. No experimental data of Flame A are shown, except for the temperature, to avoid excessive cluttering of the figure. Full symbols are used for the jet fuel doped flame (Flame B) and open symbols for the surrogate counterpart (Flame C) in this and all subsequent figures. There is virtually no distinction in the profiles of the three flames with respect to O_2, CO, CO_2 and temperature. The same consideration applies to CH_4, except at the boundary where the molar fraction has necessarily changed between Flame A and Flames B and C. Fig. 2b shows the virtually identical temperature profiles of Flames A–C. The absence of significant changes in the concentrations of CO, CO_2 and temperature due to the presence of either jet fuel or the surrogate indicates that most of these species and the heat release are produced by CH_4 oxidation. Thus, the goal of establishing a well-defined reactive environment to be slightly perturbed by either the jet fuel or its surrogate addition is achieved. Although the agreement between experiments and computational results is adequate for the present purposes, the computed CO_2 profile and temperature profile are narrower than the experimental ones, which may be due to the mismatched velocity boundary conditions, as discussed above. In view of the fact that methane accounts for the bulk of the heat release even in the doped flames, the agreement between the computational results and the experimental data in the figure is merely a reflection of the successful modeling of a CH_4 diffusion flame, which is already well established in the combustion literature.

The computational results indicate that the gas stagnation plane is at 7.6 mm from the fuel inlet, showing that the flame is positioned on the fuel side of the stagnation plane. This result is also consistent with the value of the stoichiometric mixture fraction $z_f = 0.76$ for all flames. We notice that the large stoichiometric mixture fraction, and oxygen concentration in the oxidizer stream, which were chosen to stabilize the flame in the absence of any soot [23], make these results particularly relevant to oxy-fuel combustion, which is one of the options, coupled with carbon capture and sequestration, to minimize global warming impact from combustion.

5.2. Chromatogram analysis

A lot of care must be put in the selection of the quantitation ions. When dealing with complex fuel blends as the present ones, the chromatograms tend to be noisy because of the presence of many isomers and the fact that the quantitation of compounds that can be present as different isomers (e.g., alkenes and alkylbenzenes) is often affected by the overlap of the spectra of more than one isomeric molecule in the chromatogram. Fig. 3a shows a typical jet fuel MS chromatogram from a gaseous sample extracted near the burner mouth, that is, before any significant chemistry has taken place. The arrows denote compounds that were identified and quantitated, as specified in the figure legend. The dominant peaks are associated with C9–C16 alkanes, whereas only a few of the smaller peaks, associated with the aromatics, are marked. There is a plethora of even smaller, unidentified peaks and a pedestal on which the peaks are superimposed. The final number of species we were able to measure is 30, another 20 were correctly identified but their quantitation lacks the necessary

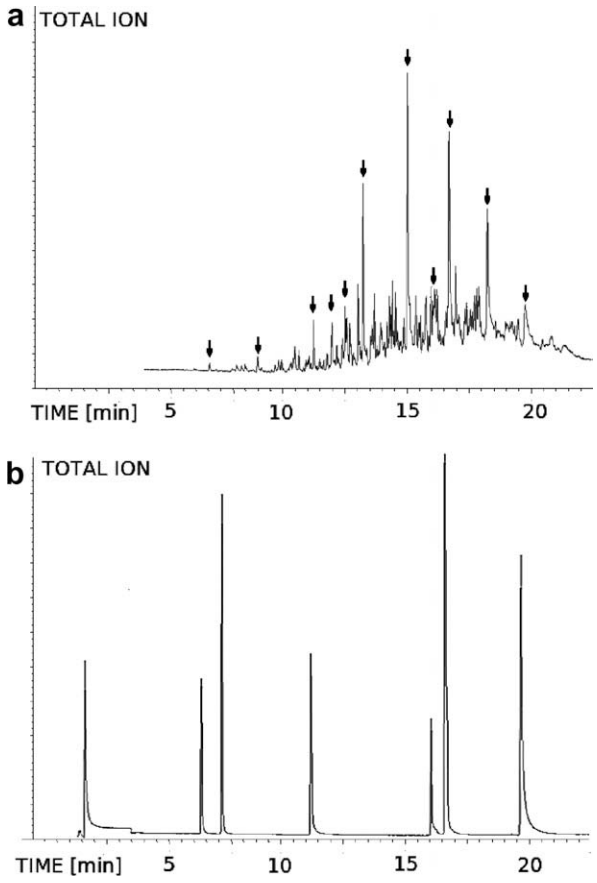

Fig. 3. (a) Typical jet fuel MS chromatogram, as measured from a gaseous sample extracted near the burner mouth. The arrows denote compounds that were identified and quantitated. From left to right: toluene, octane, *m*-xylene, nonane, 1,2,3-trimethylbenzene, decane, undecane, tetralin, dodecane, tridecane and tetradecane, respectively; (b) Jet fuel surrogate chromatogram presenting distinct peaks in correspondence with nitrogen (leftmost peak) and the 6 components of the surrogate: from left to right, methylcyclohexane, *iso*-octane, *m*-xylene, tetralin, dodecane and tetradecane.

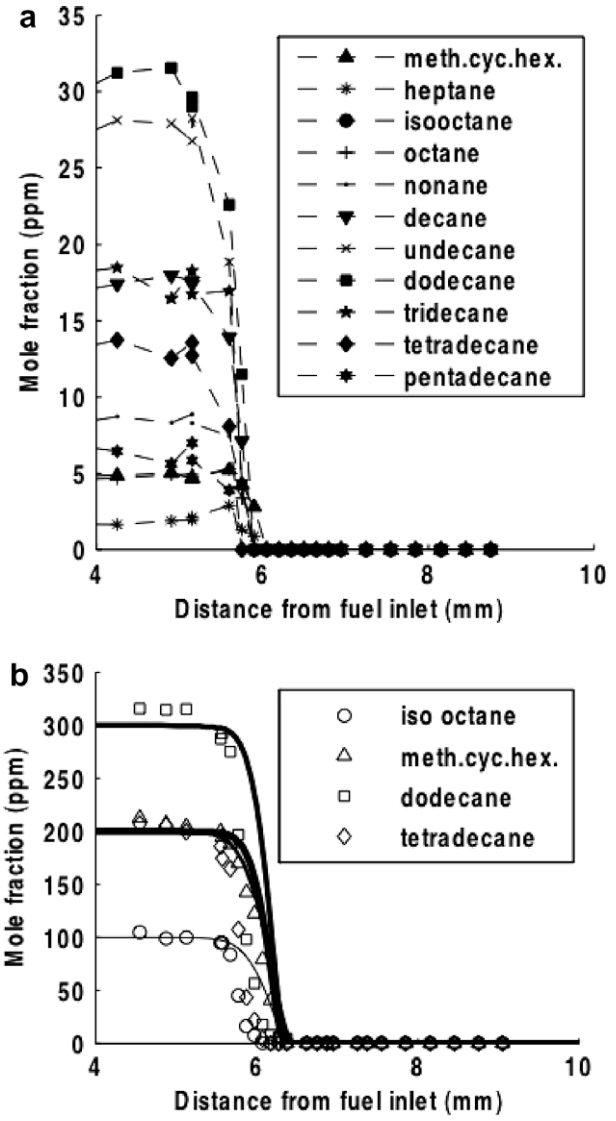

Fig. 4. Profiles of molar fractions of C7–C15 alkanes: (a) Flame B (full symbols); (b) Flame C (open symbols (experimental), solid lines (computational).

accuracy. Further refinements will be pursued in the future with the help of sensitivity studies [24] in the computational modeling to identify which minor species play a critical role from a chemical kinetic viewpoint and to develop a chemical analytical strategy to separate and quantitate them. Nevertheless, the present data are sufficient to provide a general picture of the chemical evolution in the pyrolysis and oxidation of jet fuel in a diffusion flame. By contrast, as shown in Fig. 3b, the chromatogram of the surrogate is clean and the quantitation of its components poses no difficulties. Additional considerations on the implications of the partial analysis of the jet fuel spectrum will be made with respect to the total carbon count originating from the jet fuel and the surrogate. Similar chromatograms to those in Fig. 3 were reported in [10].

5.3. C7–C15 alkanes

Fig. 4 shows the degradation of the larger, C7–C15 alkanes in the jet fuel doped flame (Flame B) (Fig. 4a) and in the surrogate flame (Flame C) (Fig. 4b). First, we notice by comparing the ordinate scales in the two figures that the sum of mole fraction values of the identified alkanes in Flame B is much smaller by comparison with the equivalent sum in Flame C. As a result, the comparison with the surrogate can be only qualitative. Yet, if the identified alkanes are regarded as tracers for a broader group of large alkanes, some useful information can be drawn. As mentioned earlier, the reason for the modest presence of alkanes in Flame B, despite the fact that they are known to be major components of the jet fuel, has to do with the complexity of the chromatogram in Fig. 3a. Jet fuel contains a large number of compounds, such as alkenes and aromatics that can have different isomers. As a result, the spectroscopic analysis presents a large "grassy" background and is very difficult to analyze. In Fig. 3a, we only considered the contribution from the major peaks (marked by arrows) that represent alkanes and some small aromatics, as indicators of a larger number of similar molecules. The presence of the pedestal prevents us from performing an accurate integration. Conversely, the chromatogram of the surrogate flame always consisted of distinct peaks that could be properly integrated, as shown in Fig. 3b. Fig. 4b shows the profiles of the same class of compounds for Flame C, along with the results of the simulation. It appears that the pyrolysis-induced disappearance of these compounds is delayed by roughly 0.3 mm in the surrogate flame. The larger alkanes exhibit a pattern roughly consistent with the disappearance of the larger and more labile hydrocarbons first, as the high-temperature region is approached. In other words, tetradecane, tridecane, dodecane, undecane, decane and nonane vanish well before the region of peak heat release and highest temperature, as marked by the CO and CO_2 profiles in

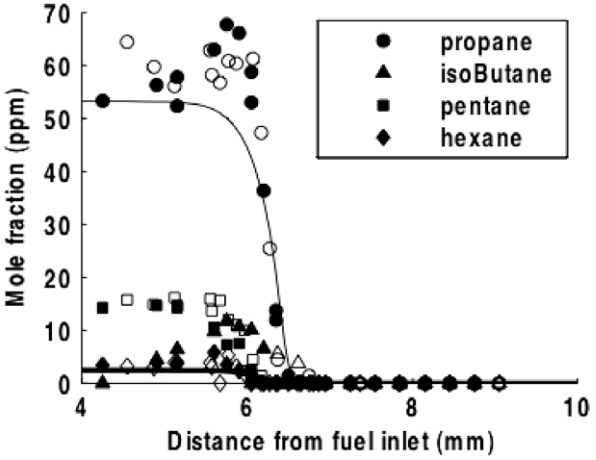

Fig. 5. Comparison of C3–C6 alkanes in Flame B (full symbols) and Flame C (open symbol (experimental), solid line (computational)).

Fig. 2. The data presented here are consistent with a typical hydrocarbon chemical kinetic pathway with large molecules decomposing thermally. The observed pattern is a consequence of the addition of jet fuel or the surrogate to the original flame and is reflective of kinetics relevant to these fuels, since the oxidation of CH_4 *per se* does not yield any of these large alkanes in detectable amounts. The data for the C7–C15 hydrocarbons show a non-monotonic behavior, with a small "hump" in the relatively colder region at $z \approx 4.0$ mm, whose nature requires further investigation. It is suspected that it may be an artifact of the long-term storage of the gas sample in the sample loop at high temperature for off-line analysis, since preliminary results with on-line analysis of the same samples do not reveal such a behavior. The well-known decomposition pathways for alkanes entails either H-atom abstraction or unimolecular dissociation to alkyl radicals, followed by beta scission of the alkyl radicals [23]. Consistent with this path, small quantities of 1-octene, 1-decene and 1-undecene and smaller alkenes were found immediately after the concentration drop of their parent alkanes. However, following the decomposition of olefines down to ethylene is extremely difficult because of the overlapping spectra of multiple isomers. Similar challenges are posed by the quantitation of dienes.

5.4. C3–C6 alkanes

Fig. 5 shows the continuous evolution of the parent alkanes leading through thermal decomposition to the formation of C3–C6 alkanes, with pentane and hexane decaying at $z \approx 6.25$ mm, and those of propane and butane at $z \approx 5.5$ mm. A comparison of the location of these peaks with that of the disappearance of the larger alkanes that starts closer to the fuel outlet further corroborates the observation that these smaller alkanes are a product of the decomposition of the larger ones. The noisy behavior of C_3H_8 is possibly related to the same gas sample storage effect discussed in connection with the "hump" in the C7–C14 profiles in the previous figure.

5.5. C2 hydrocarbons

Fig. 6 compares the measured and computed C2 species in Flames B–C. Flame C has a peak ethylene mole fraction 20% larger than Flame B, whereas the two flames seem to be in good agreement with respect to ethane and acetylene. Appearances, however, may be deceiving, since this finding may be due to the fact that a significant portion of the C2 concentrations comes from the baseline flame (Flame A). For a better defined validation of how the surrogate mimics the jet fuel behavior with respect to these species, we decided to perform the same comparison between jet fuel doping and surrogate doping in a different baseline flame with a similar temperature profile as Flame A (T_{max} = 1980 K) but with H_2 as the primary gaseous fuel, as opposed to CH_4. The molar fractions in the reactant streams for the hydrogen baseline flame were: 0.18, 0.820, 0.836 and 0.164 for H_2 and N_2 on the fuel side, and O_2 and N_2 on the oxidizer side, respectively, resulting in a stoichiometric mixture fraction $z_f = 0.856$ and an overall strain rate estimated at 112 s^{-1}. The hydrogen flame results (Fig. 6b) confirm a significant difference in ethylene mole fractions between jet fuel and surrogate, the latter presenting a lower peak concentration by about 30%. The trends for ethane and acetylene, on the other hand, are well reproduced by the surrogate with the experimental data overlapping those of the flame doped with jet fuel. A comparison with the computational results for these flames shows reasonably good agreement for ethane, but underprediction of ethylene concentration by a factor of 3 and overprediction of acetylene concentration by a similar factor in the computation.

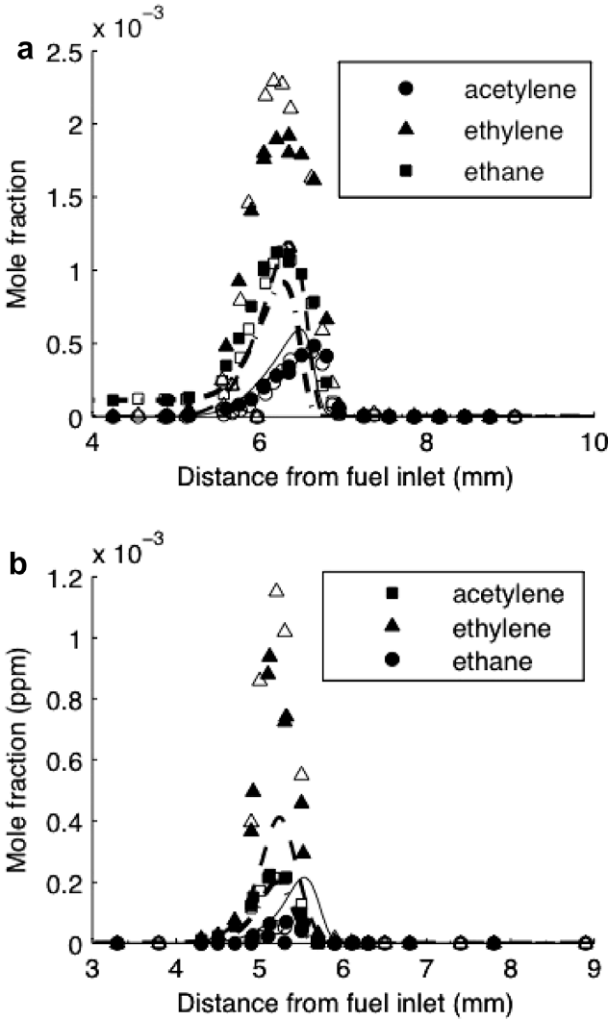

Fig. 6. Profiles of molar fractions of C2 hydrocarbons: (a) Flame B (full symbols) and Flame C (open symbols); (b) doped hydrogen flame with a similar temperature profile as in Flame A. The computed acetylene, ethylene and ethane are presented as a solid line, dashed line and dash–dot line, respectively.

5.6. Aromatics

Fig. 7a shows a comparison for some aromatics between Flames B and C, including the computational data of Flame C. There were

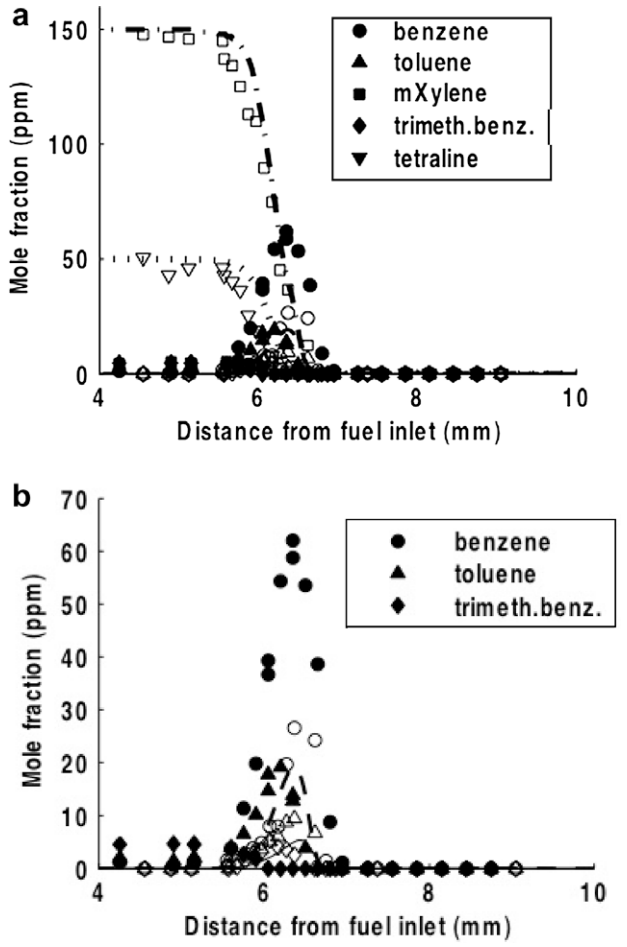

Fig. 7. Profiles of aromatics: (a) Flame B (full symbols) and Flame C (open symbols (experimental), lines (computational)); (b) enlarged view of a).

no detectable aromatics in Flame A. Therefore, the situation is clearer than for the previously discussed C2 species. *m*-Xylene, that is present in the surrogate was not detected in the jet fuel/methane flame. Tetralin was detected, but its retention time is the same as tetramethyl-benzene and was not separated. The presence of *m*-xylene and tetralin in the surrogate is meant to represent the multitude of single and multi-ring aromatics that are present in jet fuel. So, it is not surprising that there is no agreement at all between Flames B and C away from the reaction zone. More importantly, is the evolution of the aromatics within the flame. As shown in Fig. 7b that is a close-up of Fig. 7a, as the concentration of tetralin and xylene in the surrogate flame and trimethylbenzene, that is produced in small amounts in the jet fuel flame, decreases, benzene and toluene appear, with both compounds surviving the longest in the high temperature region because of their ring stabilized structure. Heavier aromatics (e.g., styrene and naphthalene) that may eventually contribute to the formation of particulates were found in even smaller quantities and are currently under investigation. The aromatic profiles exhibit the most significant difference between the jet fuel flame and the surrogate counterpart, the jet fuel flame producing much more benzene and toluene, with peak values more than a factor of two larger in Flame B as compared to Flame C. The computational model further underpredicts these species, as compared to the experimental Flame C by 20–30%. The presence of a small peak of tri-methylbenzene, that is aligned with the benzene peak, is not captured by the simulation since tri-methylbenzene does not appear as one of the species in the chemical kinetic mechanism. Significantly, even in the case of the jet fuel flame (Flame B), whose chromatogram is difficult to analyze, the error associated with the identification of these small aromatics (benzene, toluene) is very small, since they do not feature isomerism (i.e., they generate sharp, coherent peaks) and survive the early stages of oxidation (i.e., are present after the "grassy" baseline of Fig. 2 has disappeared through pyrolysis and initial oxidation). We also tested computationally a more recent surrogate formulation, Surrogate C in [5] in which the aromatics are represented by 200 ppm of *m*-xylene, with the balance of the surrogate being distributed between only *n*-dodecane (600 ppm) and methyl-cyclohexane (200 ppm). No significant improvement in the aromatic behavior was observed.

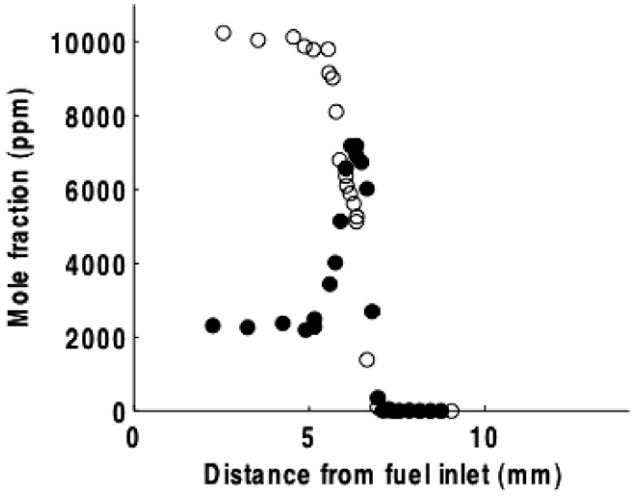

Fig. 8. Total carbon mole fraction in Flame B (full symbols) and Flame C (open symbols) (experimental), excluding the contribution from major products such as CO and CO_2, and their primary source, CH_4.

5.7. Fuel vapor carbon count

To corroborate further the quantitative nature of the data, with the exception of the C7–C15 alkanes in Fig. 4a, a comparison of the total carbon count between Flames B and C is shown in Fig. 8. The surrogate-doped flame has initially nearly 5 times as much carbon as the jet fuel doped flame. The data up to $z \approx 5$ mm show a flat profile hovering around 2200 carbon ppm for Flame B and slightly above 10,000 ppm for Flame C. The total carbon mole fraction excludes the contributions from major products such as CO and CO_2, and their primary source, CH_4 from the baseline flame (Flame A). Therefore, it should account for the fate of all the carbon generated from the parent liquid fuel to intermediate pyrolysis products. Since the overall molecular weight and flow rates of the injected vapor are comparable in the two flames, the discrepancy suggests that we properly quantitated only roughly 22% of the total carbon introduced as jet fuel vapor. Past $z \approx 5$ mm, Flame B exhibits a behavior very different from that of Flame C. In the latter, the total carbon count monotonically decreases as CO and CO_2 are formed, as shown in Fig. 2, as a consequence of the chosen definition of carbon count. At about $z \approx 7$ mm the oxidation is completed and no carbon persists in the fuel state in either flame. Conversely, in the jet fuel doped flame, after the initial plateau at 2200 ppm, the carbon count exhibits a nonmonotonic behavior, with an intermediate peak before decreasing, similar to Flame C. This behavior is a consequence of the better performance of the GC/MS in separating the jet fuel intermediate species as the largest compounds and their isomers are pyrolyzed and partially oxidized, which is consistent with the trends in the C7–C14 alkanes in Fig. 4a that were found to be in much smaller concentrations than expected. If we now revisit Fig. 7, we see that the bulk of the chemical

"action" in the formation of the small aromatics occurs between $z \approx 5.7$ mm and 6.7 mm. The consistency in total carbon count between the two flames in this region confirms the quantitative nature of the measurements of small aromatics even in the jet fuel doped flame. Therefore, only the C7–C14 alkanes in Fig. 4a are qualitative in nature and should be used for relative comparison purposes.

5.8. Probe perturbation

Probe sampling is subject to many sources of error, which can make it difficult to compare measured and computed absolute species. The potential pitfalls of sampling are comprehensively reviewed in Ref. [21] (see, also, Ref. [25]). Although the use of chemical analytical techniques to probe the pyrolysis zone of these complex hydrocarbon mixtures is virtually indispensable, a common criticism raised to these types of data is the intrusiveness of any physical probe inserted into the flame. In addition to introducing a heat sink into the combustion environments, the probe may perturb the fluid dynamics of the flame and cause systematic shifts in the position from which the sample is extracted with respect to the flame. Here we explore a procedure that assesses the intrusiveness of the probe by exploiting information from nonintrusive PLIF. Fig. 9 shows a typical signal in a jet fuel doped flame under a UV laser sheet illumination. The OH fluorescence layer in the middle of the combustion domain is separated by a thin, dark zone from a brighter region extending all the way to the fuel outlet. The latter marks the fluorescence from the aromatics contained in the fuel. These aromatics are well known to have a featureless broadband fluorescence in the visible and have been used as tracers for fuel concentration, temperature and fuel/air ratios in practical systems [26].

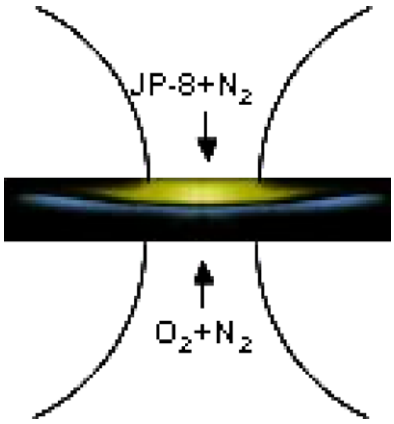

Fig. 9. PLIF of jet fuel and OH in Flame A.

Fig. 10a shows the same type of PLIF image as in Fig. 9, in the presence of the gas-sampling probe, whose silhouette is noticeable in the upper right quadrant of the picture. Both the contributions of OH and fuel sandwich a thin dark zone are still visible. However, the presence of the probe causes a "bump" in these regions. In particular, when the probe is positioned far from the stagnation plane and close to the burner mouth, the shift of the flame is more pronounced, which results in a reduction of the distance of the probe position with respect to the flame. The second and third pictures in the figure show a side-to-side comparison of the perturbed flame (Fig. 10b), with the probe axis perpendicular to the camera and the probe tip appearing as a bright, saturated spot, and the unperturbed flame (Fig. 10c). In the past, investigators typically neglected the problem and applied a systematic shift between computational and experimental studies to bring the datasets in closer agreement, as we provisionally did here. Such a procedure is in principle inaccurate, since the shift is a function of the probe position, with the most significant perturbation present when the probe is close to the burner mouth. The application of PLIF allowed us to quantify the effect of the probe intrusiveness to a position-dependent shift of at most 0.6 mm. Such a shift is considered rather modest since it amounts to approximately 10% of the physical domain where chemistry is playing a role, which corresponds to the region between 4 and 10 mm from the fuel inlet (see Fig. 2). This observation is also consistent with the results from thermocouple scans of the flames that were performed both with and without the probe in the flame, which also yielded a shift of comparable magnitude. The experimental measurements were not remapped to account for this effect, in view of the fact that the conclusions from the comparison of experiments and computational results would not be significantly affected. In summary, the 2-mm shift that was necessary to overlap experimental results and computational ones, as discussed in Section 5.1, $\sim$1 mm is due to the nitrogen shroud effect and $\leqslant$0.6 mm to the probe perturbation. The remaining discrepancy may be attributed to slightly mismatched boundary conditions in the velocity profile that may vary from plug flow to potential flow.

6. Conclusions

An experimental and computational study on the structure of a CH_4 counterflow diffusion flame doped with 1000 ppm of either jet fuel or a 6-component surrogate was successfully completed. Experimentally, the chemical analysis was performed by gas sampling through quartz microprobes and subsequent semi-automated GC/MS analysis. Conditions were chosen to ensure that all flames had identical temperature profiles and stoichiometric mixture fraction through a judicious selection of feed stream composition and strain rate. Computationally, a one-dimensional model was applied using a semi-detailed kinetic mechanism for the surrogate blend that is based on an existing hierarchically constructed kinetic model for alkanes and simple aromatics extended to

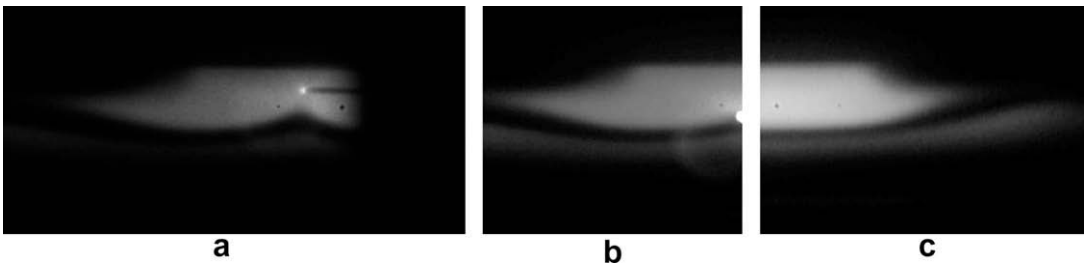

Fig. 10. PLIF of flame with intrusive effect of the gas sampling probe.

account for the presence of tetralin and methylcyclohexane as reference fuels. Principal conclusions follow:

- The experimental dataset provides a glimpse of the pyrolysis and oxidation behavior of jet fuel in a diffusion flame. The addition of the jet fuel results in the fragmentation of heavier alkanes to smaller ones, the onset of C2-hydrocarbons and the appearance of peak aromatic concentrations that are capable of withstanding higher temperatures as the location of the peak temperature is approached. This sequence is in line with the anticipated kinetic behavior, based on thermal decomposition of large alkanes to smaller and smaller fragments and the survival of ring-stabilized aromatics at higher temperatures.
- The surrogate captures this behavior reasonably well, the most significant discrepancy with respect to the jet fuel being in benzene, toluene and ethylene.
- The computational results are in reasonably good agreement with the experimental data of the surrogate-doped flame.
- A major challenge is identified in the quantification of the jet fuel components whose GC/MS analysis is at present qualitative and incomplete, as revealed by the fact that roughly only 22% of the overall carbon introduced as liquid fuel is recovered by the analysis.
- The intrusiveness of the quartz microprobe was quantified by laser-induced fluorescence visualizing the shift in OH concentration due to the presence of the probe. Such a shift was found to be at $\leqslant$0.6 mm and is considered rather modest since it amounts to approximately 10% of the physical domain where chemistry is playing a role.

Acknowledgments

The authors gratefully acknowledge the financial support of AFOSR (Grant #FA9550-06-1-0018, Dr. Julian Tishkoff, Program Manager) and of ARO (Grant # w911NF-07-1-0231, Dr. Ralph Anthenien, Program Manager); the supply of Jet A from Dr. James (Tim) Edwards (Wright–Patterson Air Force Base); the technical assistance of Dr. R.S. Tranter (Argonne National Laboratories) in the initial selection of the GC-MS configuration; and the help of Mr. N. Bernardo in the construction of the hardware.

References

[1] P. Dagaut, M. Cathonnet, Prog. Energy Combust. Sci. 32 (2006) 48.
[2] W. Shultz, ACS Petrol. Chem. Div. Preprints 37 (2) (1991) 383.
[3] A. Violi, E.G. Eddings, A.F. Sarofim, S. Granata, T. Faravelli, E. Ranzi, Combust. Sci. Tech. 174 (2002) 399.
[4] A. Agosta, N.P. Cernansky, D.L. Miller, T. Faravelli, E. Ranzi, Exp. Therm. Fluid Sci. 28 (2004) 701.
[5] S. Humer, A. Frassoldati, S. Granata, T. Faravelli, E. Ranzi, R. Seiser, K. Seshadri, Proc. Combust. Inst. 31 (2007) 393.
[6] P. Dagaut, Trans. ASME 129 (2007) 394.
[7] S. Honnet, K. Seshadri, U. Niemann, N. Peters, Proc. Comb. Inst. 32 (2009).
[8] J.A. Cooke, M. Bellucci, M.D. Smooke, A. Gomez, A. Violi, T. Faravelli, E. Ranzi, Proc. Combust. Inst. 30 (2005) 439.
[9] E. Ranzi, Energy Fuels 20 (2006) 1024.
[10] L. Tosatto, H. Bufferand, B. La Mantia, P. Duchaine, A. Gomez, Proc. Combust. Inst. 32 (2009).
[11] G. Chen, A. Gomez, Combust. Flame 110 (1997) 392.
[12] D.N. Koert, N.P. Cernansky, Meas. Sci. Technol. 3 (1992) 607.
[13] M.D. Smooke, I.K. Puri, K. Seshadri, Proc. Combust. Inst. 21 (1986) 1783.
[14] V. Giovangigli, M.D. Smooke, Combust. Sci. Tech. 53 (1987) 1.
[15] V. Giovangigli, N. Darabiha, in: C.M. Brauner, C. Schmidt-Laine (Eds.), NATO Adv. Sci. Inst. Ser. E, Martinus Nijhoff Pub., Dordrecht, 1988.
[16] R.J. Hall, J. Quant. Spectrosc. Radiat. Transfer 49 (1993) 517.
[17] D.E. Rosner, R.S. Israel, B. La Mantia, Combust. Flame 123 (2000) 547.
[18] V. Giovangigli, M.D. Smooke, J. Comp. Phys. 67 (1987) 327.
[19] V. Giovangigli, M.D. Smooke, App. Num. Math. 5 (1989).
[20] A. Hamins, D.T. Anderson, J.H. Miller, Combust. Sci. Technol. 7 (1990) 175.
[21] C. McEnally, L. Pfefferle, B. Atakan, K. Kohse-Höinghaus, Prog. Energy Combust. Sci. 30 (2004) 119.
[22] K. Seshadri, F.A. Williams, Int. J. Heat Mass Transfer 21 (2008) 251.
[23] B.M. Kumfer, S.A. Skeen, R.L. Axelbaum, Combust. Flame 154 (2008) 546.
[24] Y. Reuven, M.D. Smooke, H. Rabitz, J. Comp. Phys. 64 (1986) 27.
[25] C. McEnally, L. Pfefferle, R. Mohammed, M.D. Smooke, M.D. Colket, Anal. Chem. 71 (1999) 364.
[26] C. Schulz, V. Sick, Prog. Energy Combust. Sci. 31 (2005) 75.